Check for updates

Geochemical characteristics and oil–source rock correlation in the Paleogene source rocks of the Qinnan Sag, Bohai Bay basin

Xukai Shi [ID] and Xiaomin Xie*

The Paleogene Shahejie Formation, including the first (Es_1) and third (Es_3) members of the Shahejie Formation, and the third member of Dongying Formation (Ed_3) are important source rocks in the Qinnan Sag, Bohai Bay Basin. In order to uncover the source of oil and gas in this sag, basic geochemical, molecular geochemical, organic petrological, and n-alkane monomer carbon isotopic characteristics of source rocks and oils were analyzed in detail. In combination with the geological settings, the percentage contribution of these three sets of source rocks was assessed in the Qinnan Sag. Results obtained from the source rocks offered the following insights: (1) total organic carbon (TOC) ranged from 1.0% to 3.0%, and the S_2-TOC indicated that the qualities of source rocks followed the order of Es_3 > Es_1 > Ed_3. (2) Organic matter (OM) of the Ed_3 source rock belonged to Type II_2, while those of Es_1 and Es_3 belonged to Type II_1. The molecular geochemical parameters (CPI, $C_{24}TeT/C_{26}TT$, C_{27}–C_{29} regular steranes, and 4-MSI) also revealed that the organic matter in the source rocks mainly originated from mixtures of algae and terrestrial higher plants. (3) The % R_o values of Ed_3, Es_1, and Es_3 were 0.61%, 0.80%, and 0.88%, respectively. These results were consistent with the maturity molecular parameters (including T-max, Ts/Tm, C_{29}-$\alpha\alpha\alpha20S/(20S + 20R)$ and C_{29}-$\beta\beta/(\beta\beta + \alpha\alpha)$). (4) Pr/Ph, Pr/$nC_{17}$, and Ph/$nC_{18}$ values indicated that the three sets of source rocks were deposited in a reduced lacustrine environment with different salinities (analyzed with $G/C_{30}H$), and the salinities of Ed_3 and Es_3 indicated a freshwater brackish water environment, while that of Es_1 suggested a brackish semi-saline water environment. (5) combining the geological settings with the geochemical results of oil–source correlations, it was found that the contribution of Es_1 source rock dominated (>50%) in the sag. Overall, this study provides more accurate data of oil source formation and is significant for oil exploration in the Qinan Sag, Bohai Bay Basin.

1 Introduction

The Bohai Bay Basin, located in eastern North China, is one of the most important petroleum basins in China.[1] Depressions within the basin can be classified into three categories based on their geological history: pre-Paleogene, Paleogene, and Neogene.[2] The Qinnan Sag, positioned in the western Bohai Bay Basin, remains one of the least explored areas in the region. The discovery of the billion-ton Qinhuangdao 29 (QHD29) oilfield in 2009 stimulated intensified exploration efforts within the Qinnan Sag.

Although the tectonic framework, sedimentary characteristics, and source rock properties of the Qinnan Sag have been investigated, no significant breakthroughs have been achieved in petroleum exploration. Zhang *et al.* (2019; 2021)[3,4] investigated the QHD29 area and concluded that the formation of high-quality reservoirs in the region is mainly characterized by

three factors: rich spiral mixed beach facies, early dolomitization of buried diagenesis, and dissolution during the middle- and late-stages of diagenesis. Furthermore, they emphasized that the evolution of source rocks and modification of physical properties of the reservoir were significantly influenced by thermal fluids. Xue *et al.* (2020)[5] examined Es_1 reservoir rocks using casting sheet, scanning electron microscopy (SEM), and carbon–oxygen isotope data, revealing the widespread presence of bioclasts and emphasizing the significant influence of tectonic and sedimentary processes on reservoir quality variations. The experimental results on evaporation fractionation and biodegradation processes in the QHD29-2 oilfield demonstrate significant variations in reservoir properties between the upper and lower layers of the oil and gas reservoir.[6] Furthermore, Zhuang *et al.* (2011)[7] combined natural gas composition, isotope analysis and fluid inclusion studies, concluding that the hydrocarbons in the QHD29-2 oilfield originated from a mixture of Es_1 and Es_3 source rocks. The high-quality Paleogene source rocks in the Qinnan Sag are primarily found in the Es_3, Es_1, and Ed_3, with the southeastern subsag being particularly enriched in high-quality Es_3 and Es_1 source rocks.[8–11] The Es_3 source

Hubei Key Laboratory of Petroleum and Environmental Geochemistry (School of Resources and Environment, Yangtze University), Wuhan 430100, China. E-mail: xiaominxie2019@sina.com

rocks are characterized by high organic matter abundance, providing a solid material foundation for large-scale petroleum accumulation.[12] These findings highlight the importance of systematic geochemical characterization of source rocks and crude oil for guiding further exploration strategies.

In oil–source correlation studies, a wide range of geochemical parameters—including biomarkers and carbon isotopes—have emerged as critical tools.[13,14] Wang et al. (2015)[15] examined crude oil geochemistry and thermal maturity in the QHD29-2 oilfield using ten geochemical indicators, including 4-methylsterane (4-MSI) and gammacerane/C_{30} hopane (G/C_{30}H), based on the classification framework proposed by Hao et al. (2009).[16] Shi et al. (2022)[17] expanded the application of these indicators to both source rocks and crude oil from the eastern Qinnan Sag, evaluating geochemical traits, maturity levels, and oil–source relationships. However, due to the similarity in sterane and terpene biomarker distributions among source rocks, direct biomarker-based oil–source correlation proved inconclusive. In contrast, carbon isotope analysis has been shown to be a more reliable method for distinguishing oil sources.[18]

A multi-proxy geochemical approach was applied in this study, combining TOC analysis, rock pyrolysis, organic petrology, gas chromatography-mass spectrometry (GC-MS), and analysis of n-alkane monomer carbon isotopes. This integrated methodology was used to characterize the geochemical properties of source rocks and crude oil, establish oil–source correlations using both biomarker and isotopic evidence, and quantify the relative contributions of distinct source rock intervals to hydrocarbon generation within the Qinnan Sag. Notably, the n-alkane monomer carbon isotope composition provides critical constraints on oil–source relationships, particularly in cases where biomarker-based correlations yield ambiguous results. The findings provide new geochemical insights into source rock and crude oil characteristics in the Qinnan Sag, Bohai Bay Basin, offering valuable support for petroleum exploration and resource assessment in the region.

2 Geological overview

The Bohai Bay Basin has undergone both the Paleogene syn-rift and Neogene post-rift periods. The Qinnan Sag (Fig. 1), located in the northwestern margin of the Bohai Bay Basin, lies at the intersection of the Tanlu Fault Zone, Penglai Strike-Slip Fault Zone, and Lvshun Fault.[19] Extending in an east–west direction, the sag can be divided into four subsags from west to east: West Subsag, Middle Subsag, East Subsag, and Southeast Subsag. The structural framework of the depression is primarily controlled by the Qinnan I and Qinnan II faults, with adjacent tectonic units including the Qinnan Uplift, Liaoxi Low-Uplift, Shijiutuo Uplift, and Matouying Uplift.[20,21]

The Qinnan Sag hosts a sequence of Paleogene strata overlying the Mesozoic (Mz) basement, consisting of the Kongdian Formation (Ek), Shahejie Formation (Es), and Dongying Formation (Ed) from bottom to top.[22] The primary sedimentary systems in the Paleogene include fan deltas, braided river deltas, and lacustrine deposits. The Kongdian Formation and the Fourth Member of the Shahejie Formation were deposited under arid, oxidizing conditions, primarily forming small lacustrine or alluvial fan deposits. During the deposition of the Third Member of the Shahejie Formation, rapid subsidence created significant accommodation space. A warm and humid climate, coupled with increased precipitation, facilitated lake deepening, resulting in the extensive development of deep to semi-deep lacustrine facies, with fan delta sediments distributed along the basin margins. During the sedimentation of the First and Second Members of the Shahejie Formation, climatic conditions became slightly more arid, and fault activity weakened; however, lacustrine deposition remained dominant. In the early stages of these formations, shallow coastal lakes prevailed, whereas later stages saw lake expansion. Consequently, the depositional environment primarily consisted of shallow to semi-deep lacustrine facies, with fan deltas along the periphery and localized carbonate platform development. The Dongying Formation was influenced by strong tectonic activity and experienced a transition from lacustrine to braided river delta sedimentation. Notably, the third stage of the Dongying Formation was predominantly characterized by lacustrine deposits.[23–25]

3 Samples and experimental methods

In this study, a total of 17 crude oil samples were selected from four stratigraphic layers: Ed_3 in the Dongying Formation, Es_{12} in the Shahejie Formation, Ek in the Kongdian Formation, and Mz in the Mesozoic. Additionally, 15 source rock samples were collected from five wells across three layers: Ed_3 in the Dongying Formation, Es_1 in the Shahejie Formation, and Es_3 in the Shahejie Formation (Fig. 1).

3.1 Organic petrological analysis

This analysis includes vitrinite reflectance (R_o) measurement and maceral identification. Vitrinite reflectance (% R_o) was determined using an MSP400 microfluorescence spectrometer, applying the dual-standard calibration method (standard reference: GBW 130012), in accordance with SY/T 5124-2012. Maceral identification was performed using an MF43 transmitted polarized fluorescence microscope, equipped with a $50\times$ oil immersion objective; the specific analytical method follows the industry standard SY/T 6414-2014.

3.2 Rock pyrolysis analysis

Samples were cleaned and crushed, then 200-mesh samples were selected and analyzed with an OGE-VI Rock-Eval pyrolysis instrument.[26,27] Samples were heated to 600 °C in a helium environment, and the volatile cracking substances were carried into a hydrogen flame ionization detector (FID) through carrier gas for detection. The free hydrocarbon (S_1), residual petroleum potential (S_2), and the temperature (T-max) corresponding to the highest value of the S_2 peak, CO_2 release from organic matter (S_3), and the residual carbon content (S_4) after rock pyrolysis were detected, respectively.
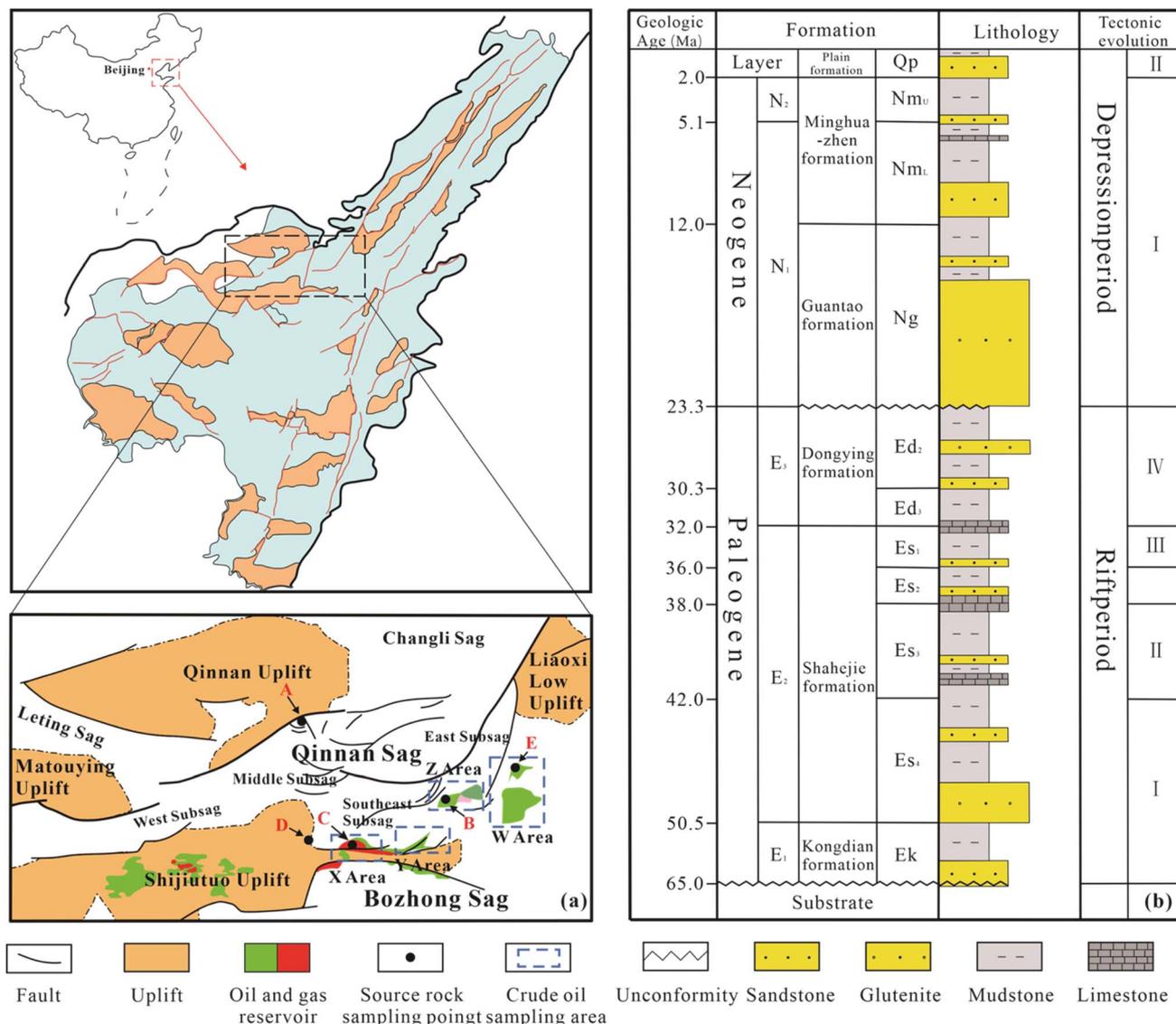
Fig. 1 (a) Simplified structural map illustrating the regional settings of the Bohai Bay Basin. The black rectangle outlines the location of the Qinnan Sag. Structural map of the Qinnan Sag showing the localities of sampling (X, Y, Z, and W areas are for crude oil sampling, and A, B, C, D, and E are for source rock sampling wells). (b) Generalized stratigraphy of the Qinnan Sag.

3.3 Total organic carbon (TOC) analysis

Samples were cleaned and crushed, then 200-mesh samples were selected and a suitable amount of powder was weighed into a crucible. The sample was treated with 1 : 7 dilute hydrochloric acid solution at 80 °C in a water bath for 12 hours to remove inorganic carbon. The sample was rinsed with ultrapure water until neutral and oven-dried. TOC content was determined using a CS-230PCHC carbon–sulfur analyzer.[26,28]

3.4 Gas chromatography-mass spectrometry (GC-MS) and pre-treatment analysis

Samples were cleaned and crushed, then 200-mesh samples were selected and extracted using Soxhlet extraction with dichloromethane as the solvent for 72 hours. Approximately

20 mg of crude oil and source rock extracts were separated into fractions using a solid-phase chromatography column packed with silica gel and alumina. Before removing asphaltenes, *n*-hexane was added, and the solution was left undisturbed for 12 hours to allow precipitation. Fractions were sequentially eluted with *n*-hexane, a 2 : 1 mixture of *n*-hexane and dichloromethane, and a 93 : 7 mixture of dichloromethane and methanol to obtain saturated hydrocarbons, aromatic hydrocarbons, and non-hydrocarbon fractions, respectively. The separated saturated hydrocarbon fraction was analyzed using an Agilent 7890B-5977B GC-MS system.[29] The chromatographic column was an HP-5MS quartz capillary column (30 m × 0.25 mm × 0.25 μm). The injector temperature was set to 300 °C, with helium as the carrier gas at a flow rate of 1 mL min^{-1}. The heating program was as follows: the initial temperature was 50 °C, held for 2

minutes, then increased at 3 °C min^{-1} to 310 °C, and held constant for 18 minutes. Electron ionization (EI) was used, with an ionization energy of 70 eV and a full mass scan range of 50–550 amu.

3.5 Carbon isotope analysis of *n*-alkane monomers

After component separation, *n*-alkanes from the crude oil and source rock extracts were subjected to monomer carbon isotope analysis.[30] The instrument used was an Isoprime (HP8890) isotope ratio mass spectrometer (IRMS), equipped with an HP-5MS quartz capillary column (30 m × 0.25 mm × 0.25 μm). The injector operated in splitless mode, with a temperature of 290 °C, using helium as the carrier gas at a flow rate of 1.0 mL min^{-1}. The temperature program was as follows: the initial temperature was 60 °C, held for 2 minutes, then ramped to 120 °C at 15 °C min^{-1}, followed by an increase to 300 °C at 4 °C min^{-1}, and held constant for 15 minutes.

4 Results

4.1 Organic petrological characteristics of source rocks

The organic matter in the source rock samples from the Qinnan Sag exhibits moderate thermal maturity, as indicated by fluorescence observed under microscopy and their evident hydrocarbon generation potential. The average vitrinite reflectance (% R_o) values for Ed$_3$, Es$_1$, and Es$_3$ are 0.61, 0.80, and 0.88,

respectively. Microscopic identification of macerals provides direct insights into the types and origins of the organic matter present in these rocks. Overall, vitrinite is abundantly developed in the Qinnan Sag source rocks, while algal content is also relatively high (Fig. 2). Well A, located in the western subsag and proximal to the provenance, is characterized by organic matter predominantly derived from terrestrial higher plants, with vitrinite as the dominant maceral component, indicative of type II$_2$–III kerogen (Fig. 2a and b). In Well D, situated on the Shijiutuo Uplift, vitrinite remains dominant in the Es$_1$ formation, while the Es$_3$ interval contains a greater proportion of aquatic algal organic matter (Fig. 2c–f). Well C, located near the deep lacustrine center, is characterized by organic matter dominated by lower aquatic organisms in both Es$_1$ and Es$_3$, with a notably higher algal contribution in Es$_3$ (Fig. 2g–l). Along a transect from Well A to Well D and then to Well C, a progressive decrease in vitrinite content and a corresponding increase in sapropelic organic matter is observed. This trend reflects the increasing distance from the provenance area and indicates an enhanced contribution from lower aquatic organisms, leading to an overall improvement in organic matter type and hydrocarbon generation potential.

4.2 Basic geochemical characteristics of source rocks

The TOC content of the source rocks follows a decreasing trend in the order of Es$_3$ (0.17–3.85%, average 1.93%) > Es$_1$ (0.34–
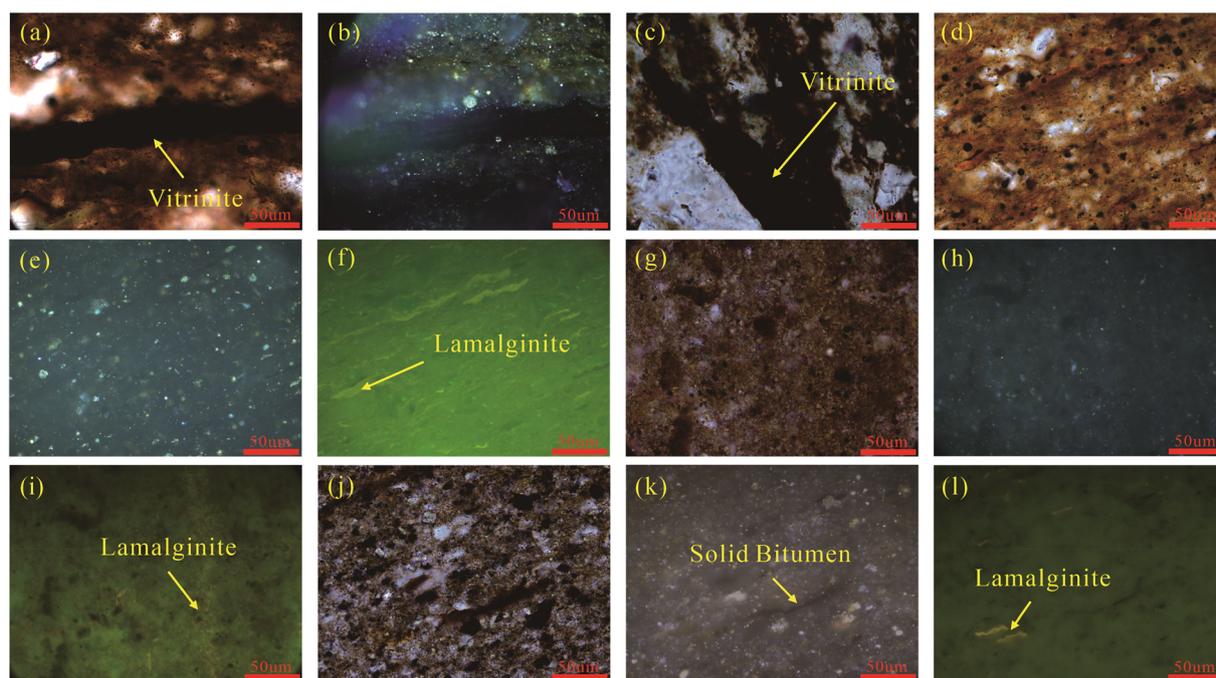

Fig. 2 Maceral identification of polished thin sections in the Qinnan sag (Scale bar = 50 μm). Note: (a) characteristics of Es$_3$ sample from Well A under transmitted light, visible development of vitrinite. (b) Characteristics of Es$_3$ sample under reflected light from Well A. (c) Characteristics of Es$_1$ sample from Well D under transmitted light, visible development of vitrinite. (d) Characteristics of Es$_3$ sample from Well D under transmitted light. (e) Characteristics of Es$_3$ sample under reflected light in Well D. (f) Fluorescence characteristics of Es$_3$ sample from Well D show the development of lamalginite. (g) Characteristics of Es$_1$ sample from Well C under transmitted light. (h) Characteristics of Well C Es$_1$ sample under reflected light. (i) Fluorescence characteristics of Es$_1$ sample from Well C show the development of lamalginite. (j) Characteristics of Es$_3$ sample from Well C under transmitted light. (k) Characteristics of Well C Es$_3$ sample under reflected light. (l) Fluorescence characteristics of Es$_3$ sample from Well C show the development of lamalginite.

2.54%, average 1.41%) > Ed$_3$ (0.30–3.00%, average 1.19%). The average values of S$_1$, S$_2$, and S$_3$ in Es$_3$ samples are 0.86 mg g^{-1}, 8.04 mg g^{-1}, and 2.13 mg g^{-1}, respectively, which are significantly higher than for other source rock layers. The average T-max value is 434 °C, with an HI range of 158–471 mg per g TOC and an average of 335 mg per g TOC, indicating a relatively good preservation of hydrogen-rich organic matter. For Es$_1$ and Ed$_3$, the average T-max values are 430 °C and 416 °C, respectively, with HI values of 207–424 mg g^{-1} and 106–300 mg per g TOC, respectively, suggesting moderate to good hydrocarbon potential. The productive carbon (PC) content in Es$_3$ ranges from 0.03% to 1.81%, higher than those of Es$_1$ and Ed$_3$ (Table 1).

4.3 Characteristics of biomarker compounds in source rocks

n-Alkanes, as dominant constituents in both source rocks and crude oils, are among the relatively early and extensively studied classes of biomarker compounds in petroleum geochemistry.[31,32] The mass fragment ion chromatograms ($m/z = 85$) of n-alkanes from source rock samples are shown in Fig. 3. The Pristane/Phytane (Pr/Ph) ratios range from 0.48 to 1.19 in the Ed$_3$ interval, 0.16 to 1.24 in Es$_1$, and 0.23 to 1.02 in Es$_3$, reflecting variations in redox conditions during sediment deposition. For isoprenoid alkanes, the Pr/nC$_{17}$ ratios in Ed$_3$, Es$_1$, and Es$_3$ are within the ranges of 0.49–0.85, 0.20–0.88, and 0.23–0.85, respectively. Meanwhile, the Ph/nC$_{18}$ ratios vary between 0.57–1.25, 0.43–1.12, and 0.56–1.30, respectively. These parameters reflect differences in depositional environments and organic matter input among the three formations. The carbon preference index (CPI) and odd–even predominance (OEP) values, used as proxies for organic matter maturity and source input, exhibit average values of 1.39, 1.63, and 1.36 for CPI, and 1.11, 1.17, and 1.20 for OEP in the Ed$_3$, Es$_1$, and Es$_3$ intervals, respectively.

The gas chromatograms of steroid and terpenoid biomarkers (Fig. 3) of three source rock samples exhibit similar characteristics: the low molecular weight tricyclic terpene shows relatively low abundance, whereas higher molecular weight hopanes and C$_{27-29}$ steranes show pronounced peaks. Selected biomarker parameters are summarized in Table 2. The ratio of C$_{24}$ tetracyclic terpenoids to C$_{26}$ tricyclic terpenoids (C$_{24}$TeT/C$_{26}$TT) falls between 0.59 and 0.76, with the ratio for occasional samples exceeding 1. The average values of $\sum w$ (tricyclic terpenes)/$\sum w$ (hopanes) for Ed$_3$, Es$_1$, and Es$_3$ are 0.22, 0.21, and 0.20, respectively. The relative ratios of C$_{27}$, C$_{28}$, and C$_{29}$ regular steranes in Ed$_3$ range from 1.52% to 36.05%, 6.95% to 18.00%, and 45.95% to 91.52%, respectively. The C$_{27}$/C$_{29}$ sterane ratios range from 0.02 to 0.78, with an average of 0.29. The relative ratios of C$_{27}$, C$_{28}$, and C$_{29}$ regular steranes in Es$_1$ range from 1.52% to 19.83%, 4.91% to 27.82%, and 57.53% to 90.07%, respectively, with C$_{27}$/C$_{29}$ ratios ranging from 0.02 to 0.33 (average 0.13). In Es$_3$, the C$_{27}$, C$_{28}$, and C$_{29}$ steranes range from 3.62% to 23.92%, 6.86% to 14.14%, and 64.79% to 88.60%, respectively, with C$_{27}$/C$_{29}$ ratio ranges from 0.04 to 0.35, averaging 0.19. All formations display a predominance of C$_{29}$ steranes, consistent with higher plant-derived organic matter input. The abundance of tetramethylsterane (4-MSI) ranges from 0.06 to 0.33 in Ed$_3$, 0.07 to 0.33 in Es$_1$, and 0.06 to 0.35 in Es$_3$.

4.4 Characteristics of biomarker compounds in crude oil

The n-alkane series in crude oil samples is relatively complete and exhibits a predominantly unimodal distribution. The analysis of saturated hydrocarbons (Table 2) shows that the Pr/Ph ratios in all samples are below 1. Specifically, the Pr/Ph values range from 0.66 to 0.82 in Ed$_3$ (average: 0.75), 0.46 to 0.91 in Es$_{12}$ (average: 0.70), 0.70 to 0.86 in Ek (average: 0.78), and 0.47 to 0.89 in Mz (average: 0.72). The average CPI values for Ed$_3$, Es$_{12}$, Ek, and Mz are 1.09, 1.12, 1.10, and 1.10, respectively, while their OEP values are 1.06, 1.07, 1.09, and 1.10, respectively. For isoprenoid alkanes, Pr/nC$_{17}$ values generally range from 0.19 to 0.63, while most Ph/nC$_{18}$ values fall between 0.20 and 1.28.

Table 1 Basic geochemical parameters of source rocks in the Qinnan Sag[a]

Number	Sampling	Depth (m)	Layer	S$_1$ (mg g^{-1})	S$_2$ (mg g^{-1})	S$_3$ (mg g^{-1})	T-max (°C)	S$_1$ + S$_2$ (mg g^{-1})	S$_4$ (mg g^{-1})	TOC (%)	PI	HI (mg g^{-1})	PC (%)
S-1	A	2630	Ed$_3$	0.09	0.46	1.13	409	0.55	2.10	0.30	0.16	153	0.09
S-2		2875	Es$_1$	0.16	1.14	0.98	431	1.30	4.00	0.55	0.13	207	0.15
S-3		2935	Es$_1$	0.13	1.34	1.30	429	1.47	1.60	0.34	0.09	394	0.18
S-4	B	3014	Es$_1$	0.12	4.70	1.4	434	4.82	13.20	1.72	0.02	273	0.4
S-5		3062	Es$_1$	0.17	4.14	1.22	435	4.31	11.20	1.48	0.03	279	0.35
S-6		3096	Es$_3$	0.10	3.96	1.94	433	4.06	9.50	1.36	0.02	291	0.41
S-7	C	3330	Ed$_3$	0.54	1.65	1.85	404	2.19	2.90	0.55	0.25	300	0.26
S-8		3605	Es$_1$	0.82	10.91	3.07	442	11.73	15.70	2.54	0.07	431	0.98
S-9		3660	Es$_3$	0.74	9.79	3.72	440	10.53	14.70	2.34	0.07	420	0.88
S-10	D	2930	Ed$_3$	0.21	1.55	2.44	406	1.76	5.90	0.83	0.12	187	0.24
S-11		3160	Es$_1$	0.28	2.50	2.00	417	2.78	4.50	0.76	0.10	329	0.31
S-12		3320	Es$_3$	2.49	18.14	1.85	436	20.63	20.40	3.85	0.12	471	1.81
S-13	E	3110	Ed$_3$	0.30	3.26	1.32	445	3.57	27.78	3.07	0.09	106	0.30
S-14		3150	Es$_1$	0.61	10.58	2.87	442	11.19	15.68	2.50	0.05	424	0.93
S-15		3290	Es$_3$	0.11	0.27	1.01	425	0.37	1.36	0.17	0.29	158	0.03

[a] S = source rock; S$_1$ = free hydrocarbon; S$_2$ = residual petroleum potential; S$_3$ = CO$_2$ release from organic matter; S$_4$ = residual carbon after cracking; T-max = S$_2$ peak temperature; TOC = total organic carbon; PI = S$_1$/(S$_1$ + S$_2$); HI = S$_2$ × 100/TOC; PC = 0.083 × (S$_1$ + S$_2$).
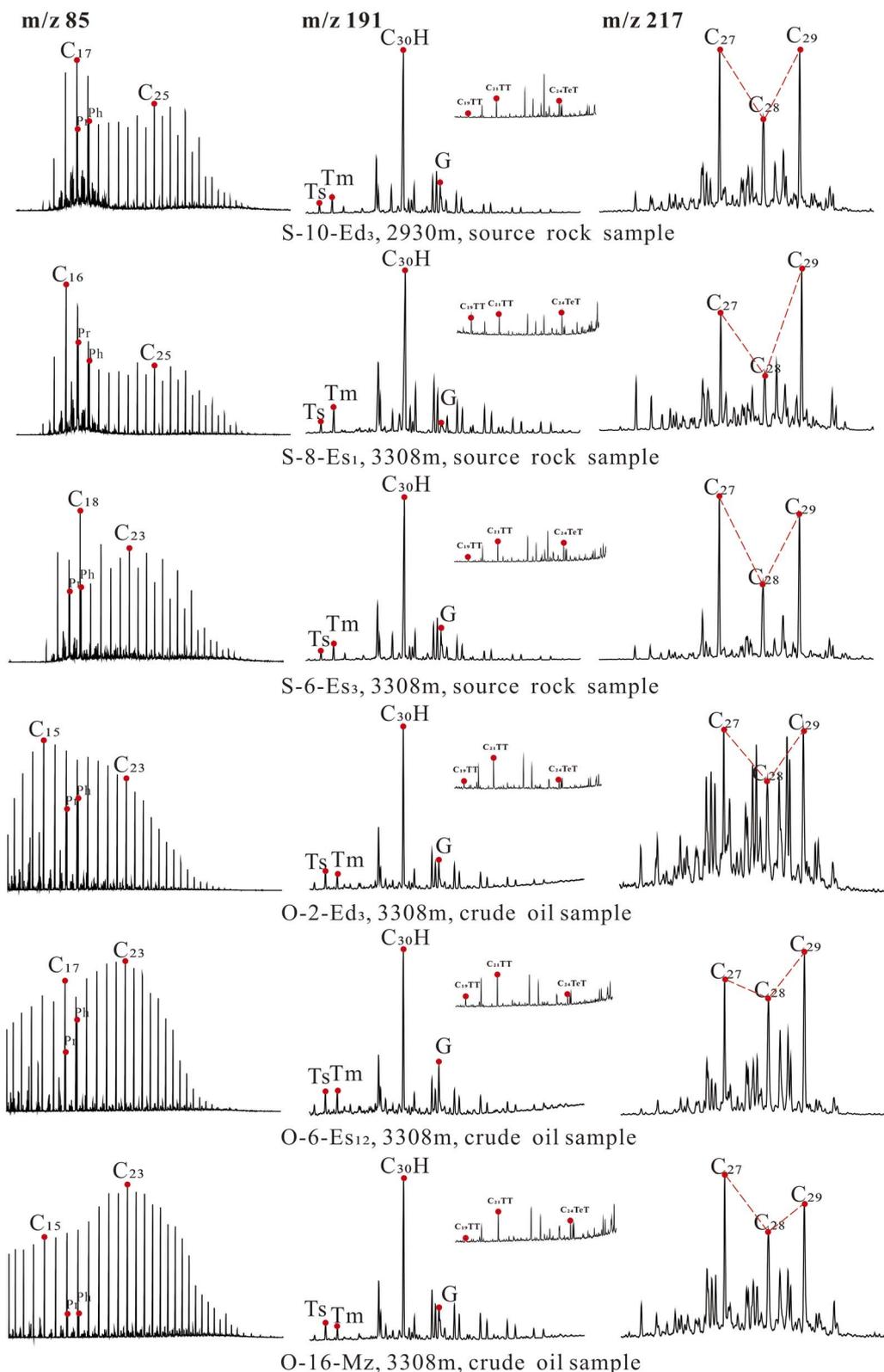
Fig. 3 Distribution characteristics of n-alkane, terpene and sterane series in different layers of source rocks and crude oil in the Qinnan Sag (m/z = 85, m/z = 191, m/z = 217).

The sterane and terpane biomarkers in the crude oil exhibit compositional characteristics similar to those observed in the source rocks. Low-molecular-weight tricyclic terpenes are present in low abundance, with the $\sum w$ (tricyclic terpenes)/$\sum w$ (hopanes) ratio primarily ranging from 0.12 to 0.61. In contrast, high-molecular-weight hopanes and C_{27-29} regular steranes are

Table 2 n-Alkane series and common terpene and sterane parameters in source rock and crude oil of different layers in the Qinnan Sag[a]

Number	Sampling	Layer	Depth (m)	CPI	OEP	Pr/nC_{17}	Ph/nC_{18}	Pr/Ph	nC_{21}/$nC_{22}+$	$C_{19}T$/$C_{23}T$	$C_{23}T$/$C_{30}H$	$C_{24}Te$/$C_{26}T$	Ts/Tm	$C_{29}Ts$/$C_{29}H$	$diaC_{27}$/$diaC_{29}$	$diaC_{29}$/reC_{29}	C_{29} sterane 20S/(20S + 20R)	C_{29} sterane $\beta\beta$/($\alpha\alpha$ + $\beta\beta$)	G/$C_{30}H$	4-MSI
O-1	X area	Ed_3	3301	1.10	1.07	0.36	0.56	0.66	0.98	0.21	0.03	0.51	0.93	0.40	0.98	0.19	0.48	0.59	0.19	0.32
O-2		Ed_3	3195	1.11	1.06	0.39	0.58	0.76	1.11	0.46	0.14	0.59	1.10	0.47	1.40	0.24	0.49	0.61	0.32	0.24
O-3	Y Area	Es_{12}	3175	1.17	1.05	0.32	0.43	0.89	1.18	0.44	0.26	0.48	1.68	0.45	1.46	0.31	0.50	0.62	0.39	0.20
O-4		Es_{12}	3280	1.08	1.05	0.30	0.44	0.69	0.96	0.36	0.09	0.44	1.43	0.54	1.49	0.21	0.50	0.63	0.35	0.27
O-5		Es_{12}	3495	1.09	1.06	0.49	1.14	0.51	0.97	0.36	0.08	0.51	0.75	0.39	1.32	0.19	0.49	0.64	0.43	0.17
O-6		Es_{12}	3308	1.10	1.04	0.42	0.87	0.55	0.97	0.47	0.13	0.50	1.11	0.46	1.15	0.23	0.51	0.64	0.47	0.17
O-7		Es_{12}	3475	1.12	1.08	0.48	1.28	0.46	0.97	0.26	0.03	0.53	0.60	0.30	0.94	0.14	0.43	0.47	0.39	0.14
O-8		Es_{12}	3390	1.19	1.13	0.45	0.70	0.67	0.99	0.22	0.04	0.52	0.71	0.34	1.18	0.22	0.36	0.36	0.24	0.39
O-9	Z area	Mz	3388	1.13	1.10	0.63	1.21	0.47	0.96	0.16	0.03	0.66	0.81	0.28	0.75	0.15	0.43	0.52	0.35	0.15
O-10		Es_{12}	2747	1.16	1.06	0.32	0.44	0.82	1.26	0.29	0.08	0.42	1.02	0.39	2.58	0.14	0.41	0.53	0.30	0.35
O-11		Ek	2938	1.09	1.01	0.32	0.43	0.70	1.43	0.60	0.03	0.71	0.58	0.29	1.62	0.11	0.44	0.53	0.24	0.16
O-12	W area	Ed_3	3065	1.06	1.05	0.24	0.28	0.82	1.00	0.20	0.07	0.41	1.15	0.49	1.51	0.22	0.48	0.59	0.49	0.26
O-13		Es_{12}	3167	1.10	1.07	0.23	0.24	0.91	1.01	0.46	0.14	0.59	1.10	0.47	1.40	0.24	0.39	0.49	0.32	0.52
O-14		Es_{12}	3282	1.06	1.07	0.24	0.29	0.77	0.97	0.27	0.04	0.56	1.28	0.42	1.07	0.22	0.46	0.51	0.46	0.27
O-15		Mz	3401	1.09	1.06	0.24	0.29	0.79	0.96	0.25	0.05	0.56	1.28	0.56	1.78	0.17	0.50	0.53	0.33	0.28
O-16		Mz	3400	1.09	1.06	0.19	0.20	0.89	0.95	0.20	0.04	0.51	1.23	0.50	1.92	0.15	0.40	0.43	0.24	0.26
O-17		Ek	3187	1.12	1.16	2.91	4.00	0.86	0.89	0.16	0.08	0.40	1.08	0.42	1.29	0.26	0.53	0.64	0.40	0.50
S-1	A	Ed_3	2630	1.24	1.03	0.85	1.26	0.48	0.54	0.09	0.33	0.64	0.92	8.69	1.13	0.38	0.45	0.41	0.09	0.33
S-2		Es_{12}	2875	1.19	1.03	0.88	1.12	0.52	0.64	0.02	0.13	1.06	0.47	1.90	0.51	0.50	0.40	0.21	0.32	0.29
S-3		Es_{12}	2935	1.75	1.08	0.82	1.02	0.78	0.55	0.26	0.46	0.64	0.89	0.36	0.92	0.59	0.36	0.39	0.16	0.15
S-4	B	Es_{12}	3014	2.18	1.27	0.20	0.43	0.17	0.97	0.25	0.01	1.29	0.57	0.34	1.44	0.11	0.65	0.40	0.08	0.07
S-5		Es_{12}	3062	2.10	1.39	0.21	0.55	0.16	1.11	0.27	0.01	1.01	0.59	0.32	0.25	0.62	0.69	0.29	0.24	0.10
S-6		Es_3	3096	1.46	1.15	0.23	0.56	0.23	0.87	0.21	0.02	0.66	0.66	0.44	0.29	0.59	0.53	0.35	0.25	0.13
S-7	C	Ed_3	3330	1.20	1.12	0.54	0.84	0.86	0.87	0.27	0.04	0.59	0.56	0.36	0.19	0.92	0.42	0.57	0.49	0.06
S-8		Es_{12}	3605	1.34	1.23	0.56	0.87	1.25	1.06	0.96	0.01	1.23	0.48	0.34	0.67	0.50	0.48	0.68	0.05	0.13
S-9		Es_3	3660	1.42	1.29	0.51	1.01	1.03	0.99	0.36	0.01	1.75	0.61	0.38	0.53	0.41	0.48	0.62	0.03	0.06
S-10	D	Ed_3	2930	1.45	1.15	0.54	0.89	0.76	1.07	0.09	0.04	0.75	0.56	0.39	0.35	0.41	0.48	0.51	0.23	0.12
S-11		Es_{12}	3160	1.49	1.04	0.60	0.80	0.98	1.07	0.62	0.04	0.72	0.70	0.48	0.25	0.77	0.47	0.50	0.73	0.27
S-12		Es_3	3320	1.27	1.24	0.84	1.30	0.56	1.03	0.18	0.01	0.74	0.63	0.25	0.45	0.49	0.68	0.48	0.04	0.28
S-13	E	Ed_3	3110	1.69	1.13	0.49	0.57	1.19	1.07	0.16	0.03	0.76	0.41	0.52	0.40	0.57	0.55	0.41	0.08	0.10
S-14		Es_{12}	3150	1.39	1.17	0.62	0.93	0.90	0.86	0.25	0.06	0.76	0.55	0.47	0.10	0.96	0.33	0.41	0.35	0.32
S-15		Es_3	3290	1.28	1.10	0.41	0.59	0.51	0.66	0.03	0.57	0.67	0.83	0.44	0.32	0.81	0.60	0.51	0.13	0.35

[a] O = oil sample; S = source rock sample; CPI = {($C_{25} + C_{27} + C_{29} + C_{31} + C_{33}$)[1/($C_{24} + C_{26} + C_{28} + C_{30} + C_{32} + C_{34}$)] + 1/($C_{26} + C_{28} + C_{30} + C_{32} + C_{34}$)]}/2; OEP = [($C_i + 6 C_{i+2} + C_{i+4}$)/4($C_{i+1} + C_{i+3}$)]^m, where m = $(-1)^{i+1}$, $i + 2$ is the carbon number of the main peak; Pr = pristane; Ph = phytane; n = n-alkanes; T = tricyclic terpene; H = hopane; Te = tetracyclic terpenes; Ts = 18α(H)-trisnorhopane; Tm = 17α(H)-trisnorhopane; dia = diasterane; re = regular sterane; G = gammacerane.
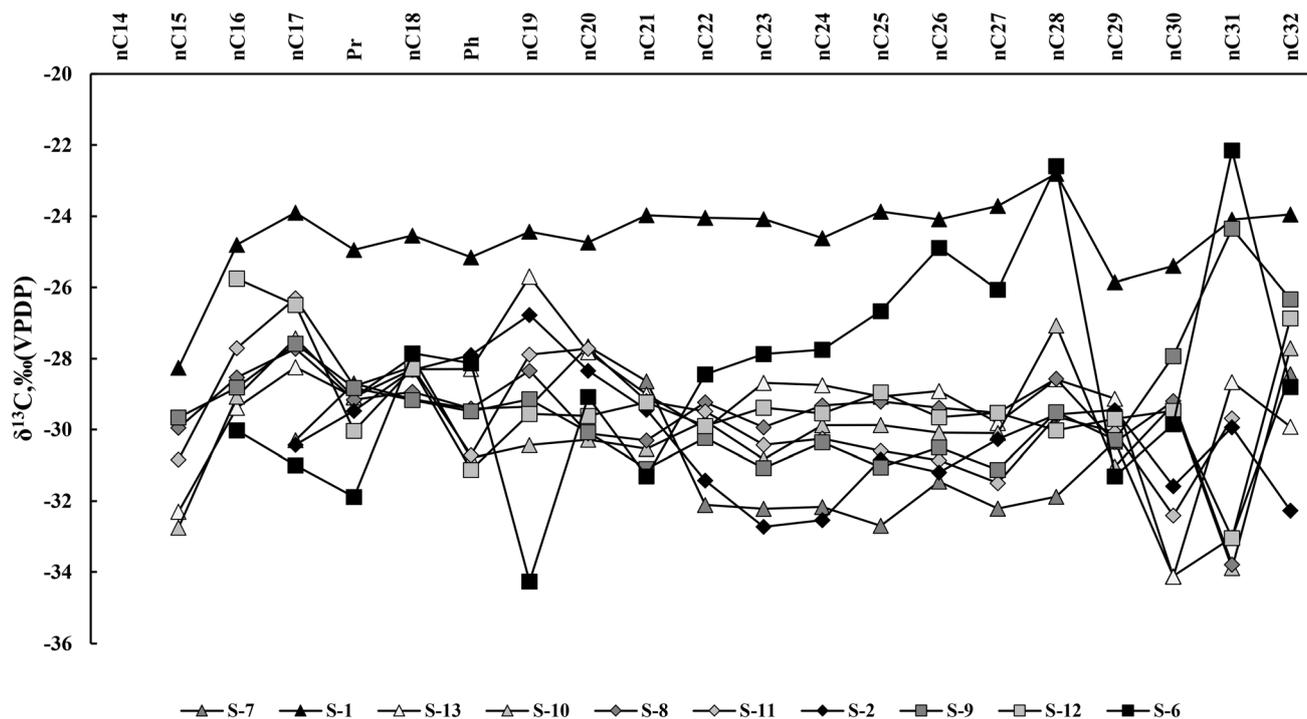
Fig. 4 Carbon isotope characteristics of *n*-alkane monomers of source rocks in the Qinnan Sag.

relatively enriched. The relative proportions of C_{27}, C_{28}, and C_{29} regular steranes range from 0.16–0.33%, 0.31–0.60%, and 0.11–0.46%, respectively. The C_{27}/C_{29} sterane ratio varies from 0.38 to 2.60, with an average of 0.75, indicating a predominance of C_{29} steranes. Table 2 indicates that the terpenoid biomarker parameters of crude oil samples are relatively concentrated. The $C_{24}TeT/C_{26}TT$ ratio, an indicator of higher plant input, is relatively low and shows a marked contrast with that observed in the Es_3 section. The $G/C_{30}H$ ratio ranges from 0.19 to 0.46, with an average of 0.35. The 4-MSI ratio ranges from 0.14 to 0.50.

Fig. 5 Carbon isotope characteristics of *n*-alkane monomers of crude oils in the Qinnan Sag.

4.5 Monomer carbon isotope characteristics of *n*-alkanes in source rocks and crude oil

n-Alkane monomer carbon isotopic analysis (δ^{13}C) was conducted to investigate the genetic relationship between source rocks and crude oils in the Qinnan Sag. The analysis focused on *n*-alkanes ranging from nC$_{14}$–nC$_{32}$ and Pr and Ph data. The δ^{13}C values for crude oil (Fig. 4) ranged from −30‰ to −24‰, with an average of −28.02‰. The δ^{13}C values of the source rocks (Fig. 5) ranged from −30‰ to −26‰, with an average of −29.41‰. A few samples exhibited δ^{13}C values ranging from −30‰ to −24‰. Crude oils exhibited more enriched and consistent δ^{13}C values than the source rocks. Due to abnormal δ^{13}C signatures observed in Ek crude oil samples, these were excluded from subsequent oil–source correlation analyses.

5 Discussion

5.1 Type and maturity

The hydrocarbon generation potential of source rocks should be evaluated based on the organic matter type and maturity.[33–35] The kerogen type classification diagram based on T-max *versus* HI (Fig. 6a) indicates that Es$_3$ samples fall within Type II$_1$, Ed$_3$ samples in Type II$_2$, and Es$_1$ samples in Type II$_1$. Microscopic composition analysis (Fig. 2) further supports these classifications. The T-max data indicate that the source rocks in the Qinnan Sag are distributed from immature to maturity stages.

Combined with the % R_o data, it can be concluded that Es$_1$ and Es$_3$ exhibit characteristics of low to moderate maturity, while Ed$_3$ exhibits immature to low maturity stages.[36]

In terms of biomarker-based maturity parameters, the thermal evolution trends reflected by individual indicators are broadly consistent. It is generally believed that with increasing maturity, Tm gradually transforms into Ts, causing Ts/Tm to increase.[37] As shown in Fig. 6b, the mean value of Es$_3$ in source rocks is higher than those of Es$_1$ and Ed$_3$, indicating a greater thermal maturity. The Ts/Tm values in crude oil samples are generally above 1, reflecting their overall higher maturity, which suggests that Ed$_3$ source rocks may have made only a limited contribution to oil generation. The isomerization ratios of C$_{29}$ steranes, such as C$_{29}$-$\alpha\alpha\alpha$20S/(20S + 20R) and C$_{29}\beta\beta$/($\beta\beta$ + $\alpha\alpha$), are also widely used as maturity indicators.[38] With thermal evolution, α-type steranes convert into β-types, and the biological configuration (20R) shifts toward the geological equilibrium configuration (20S), resulting in increased ratios.[39] In both source rock and crude oil samples, the C$_{29}$-$\alpha\alpha\alpha$20S/(20S + 20R) and C$_{29}\beta\beta$/($\beta\beta$ + $\alpha\alpha$) values cluster around 0.5 and 0.6 (Fig. 6c), indicating that these samples have reached isomerization equilibrium.[30] Consequently, these parameters are less effective for further maturity discrimination among crude oil samples. Based on the above data and the distribution map of S$_2$-TOC (Fig. 6d), it can be concluded that Es$_3$ is a high-quality source rock and Es$_1$ is the least favorable in terms of hydrocarbon generation potential.
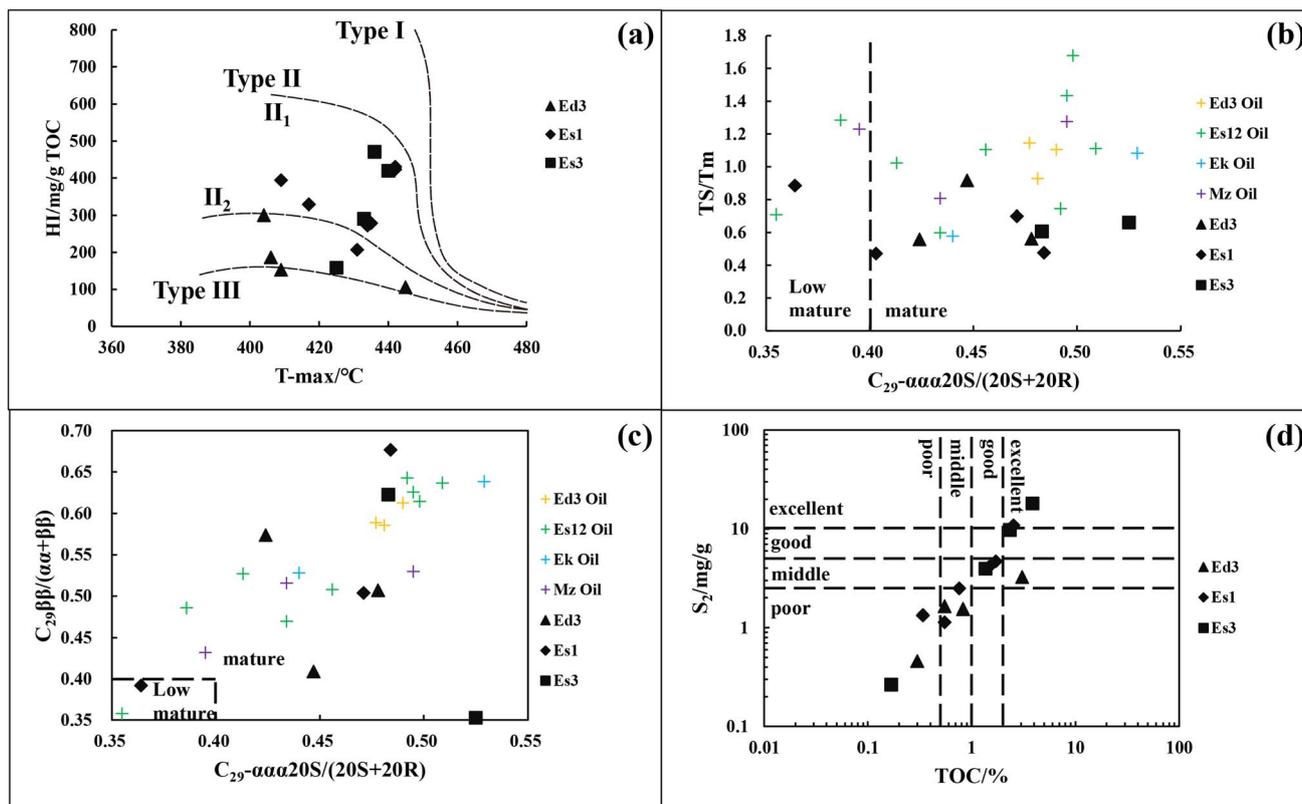

Fig. 6 T-Max-HI values of (a), Ts/Tm-C$_{29}$20S/(20S + 20R) (b), C$_{29}\beta\beta$/($\alpha\alpha$ + $\beta\beta$)−C$_{29}$20S/(20S + 20R) (c), and S$_2$-TOC (d) classification diagrams of source rock and crude oil in the Qinnan Sag.

5.2 Source of parent material and sedimentary environment

The nature of the parent material plays a decisive role in determining both the type and hydrocarbon generation potential of source rocks. Biomarkers such as peak carbon number, CPI values, $C_{19}TT/C_{23}TT$, $C_{24}TeT/C_{26}TT$, C_{27}–C_{29} regular steranes, and 4-MSI index are commonly used as indicators of organic input and depositional settings.

Biomarker analysis of source rock samples from the Qinnan Sag shows that the *n*-alkane series in most samples exhibited a bimodal pattern, with two distinct peak groups.[18] In these bimodal distributions, the first peak typically centers around nC_{16}, while the second peak is generally observed near nC_{25}. This pattern reflects the relatively small loss of low molecular weight compounds and suggests a mixed origin of organic matter. The intervening trough between the two peaks generally appears at nC_{21} or nC_{22}, exhibiting a weak odd-carbon preference. However, this feature is relatively insignificant when compared to the pronounced odd–even predominance typically observed in terrestrial plant and modern surface sediments.[28] Based on multiple geochemical indicators—including $C_{24}TeT/C_{26}TT$, the distribution of C_{27}–C_{29} regular steranes, and molecular composition characteristics—it is inferred that the source rocks contain a mixed organic input derived from both lower aquatic organisms (*e.g.*, algae) and terrestrial higher plants. In contrast, the *n*-alkane distribution in crude oil samples is relatively complete and predominantly unimodal, although both front and rear peak types are present, suggesting varying contributions from different biogenic sources. CPI and OEP values close to 1 indicate no significant odd–even preference, further supporting the thermal maturity and absence of recent terrestrial contamination. Taking into account biomarker parameters such as $C_{24}TeT/C_{26}TT$ and sterane distribution, the crude oil is believed to originate from a mixed source dominated by algal input.

Pr/Ph ratios are widely recognized as proxies for redox conditions, while Pr/nC_{17} and Ph/nC_{18} ratios are commonly used to evaluate both the sedimentary environment and organic matter input.[39–41] Stratigraphic comparison of source rock samples indicates that Ed_3, Es_1, and Es_3 were all deposited

under reducing conditions, as suggested by the low Pr/Ph values (Fig. 7a). The Pr/nC_{17} and Ph/nC_{18} ratios also indicate the characteristics of their lacustrine sedimentary environment, and their organic matter types are consistent with *T*-max-HI, confirming that the parent material of the crude oil was derived from a relatively reducing lacustrine environment (Fig. 7b).

Gammacerane, a pentacyclic triterpenoid, is generally formed *via* the reduction of tetracyclic alcohols in protozoa and photosynthetic bacteria, and its presence is closely linked to the depositional environment. Elevated gammacerane concentrations are typically associated with strongly reducing, stratified, and saline water bodies. The gammacerane index ($G/C_{30}H$) is commonly used to assess salinity: values above 0.2 are generally indicative of brackish to saline depositional conditions and can be used as a marker for water stratification.[27] In the Qinnan Sag, Ed_3 and Es_3 source rocks were deposited in freshwater to brackish water settings, while Es_1 reflects a brackish to semi-saline environment. The crude oil samples are interpreted to have formed in saline to slightly saline conditions (Fig. 7a).

5.3 Oil–source rock correlation

Oil–source rock correlation integrates geological context with geochemical data to evaluate the genetic relationships between crude oils and potential source rocks. A wide array of geochemical indicators are typically employed in such analyses, including crude oil physical properties, bulk compositions, biomarker compounds, and stable carbon isotopes.[42] However, each parameter has specific limitations and applicable conditions.[43–45] It is generally necessary to integrate various parameters for geochemical correlation so that the results are more reliable. Traditional oil–source correlation relies on comparing the geochemical characteristics of oils and source rocks to infer shared origins. For example, *n*-alkanes, tricyclic terpenes, tetracyclic terpenes, C_{30} hopane, and C_{27}, C_{28}, C_{29} regular steranes are used to analyze the sources of bacteria, algae, and higher plants.[46–49] Exploring thermal maturity using Ts/Tm, C_{29}-$\alpha\alpha\alpha20S/(20S + 20R)$ and $C_{29}\beta\beta/(\beta\beta + \alpha\alpha)$.[50–52] Pr/nC_{17}, Ph/nC_{18}, and gammacerane indicate sedimentary redox
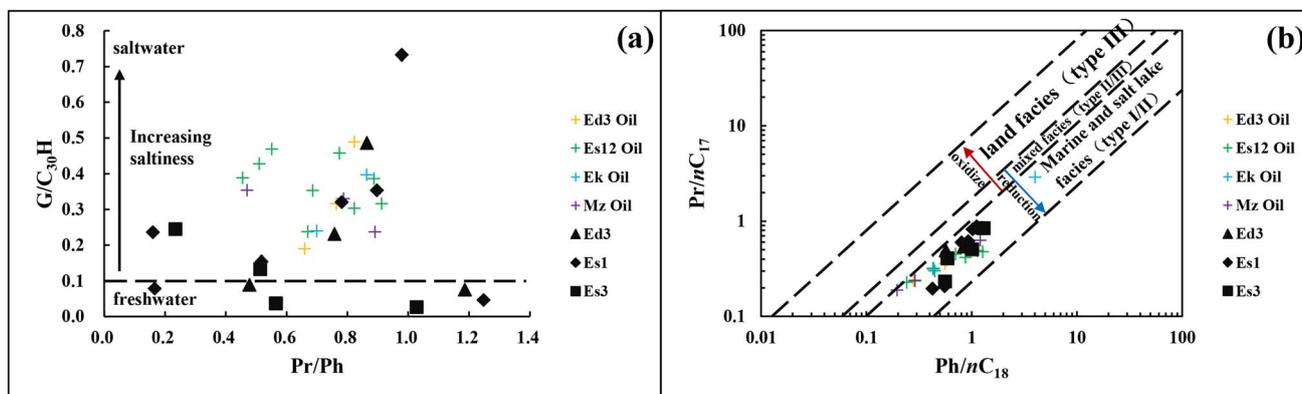

Fig. 7 Analysis of the relationship between Pr/Ph and $G/C_{30}H$ (a) and Pr/nC_{17} and Ph/nC_{18} (b) values in source rocks and crude oil of the Qinnan Sag.

conditions and salinity levels.[53–55] Previous studies in the Bohai Bay Basin[56] identified 4-MSI as a key biomarker for oil–source correlation. This compound is typically derived from 4α-methylsterols produced by dinoflagellates, although it may also originate from certain bacteria.[56] Hao *et al.* (2009)[16] utilized 4-MSI as a key indicator for oil source analysis in the Bozhong Depression and Shijiutuo Uplift. Wang *et al.* (2015)[15] used the parameters from Hao *et al.* (2009)[16] to conduct cluster analysis on the QHD29 oilfield, which effectively identified the oil source information of crude oil. However, Shi *et al.* (2022)[17] compared crude oil and source rock characteristics in the eastern part of Qinnan using indicators such as 4MSI and G/C_{30} hopane and found that the application of the biomarker compound characteristic by Hao *et al.* (2009)[16] in the Qinnan area presents certain limitations. The high similarity of sterane and terpene biomarkers in source rocks reduces the significance of parameter-based comparisons, resulting in unclear oil–source correlation outcomes. These findings suggest that, in the Qinnan Sag, biomarker-based approaches alone are insufficient for reliable oil–source correlation, and that alternative methods are required to improve the accuracy of oil–source identification.

Previous studies[18,57] have found that, despite similar biomarker distributions, significant distinctions arise when comparing carbon isotopic signatures. δ^{13}C values of sedimentary organic matter primarily reflect the carbon isotope composition of its biological precursors.[58,59] Unlike biomarkers, monomer carbon isotopes are less affected by biodegradation or migration, making them more reliable indicators of source input and depositional environment. However, direct oil–source comparison between crude oil and over-mature source rocks should be avoided. Compared to group component carbon isotopes, monomer carbon isotopes provide more refined results and enable source analysis at a finer molecular level.[60] Therefore, this study employs *n*-alkane monomer carbon isotopes for oil–source correlation analysis.

The *n*-alkane carbon isotope results from 15 source rock samples in the Qinnan Sag reveal distinct isotopic differences across different stratigraphic intervals. After eliminating incomplete and anomalous data, 10 representative samples from three different layers were selected for further analysis (Fig. 8). Isotopic differentiation is mainly observed in three aspects: (a) the δ^{13}C values of light *n*-alkanes with carbon numbers below 17, (b) correlations between nC_{17}–nC_{19} and isoprenoids (Pr and Ph), and (c) variations in the δ^{13}C values of heavy *n*-alkanes with carbon numbers above 20.

From the distribution of *n*-alkane monomer carbon isotopes in the source rocks (Fig. 8), the Ed_3 formation exhibits notable
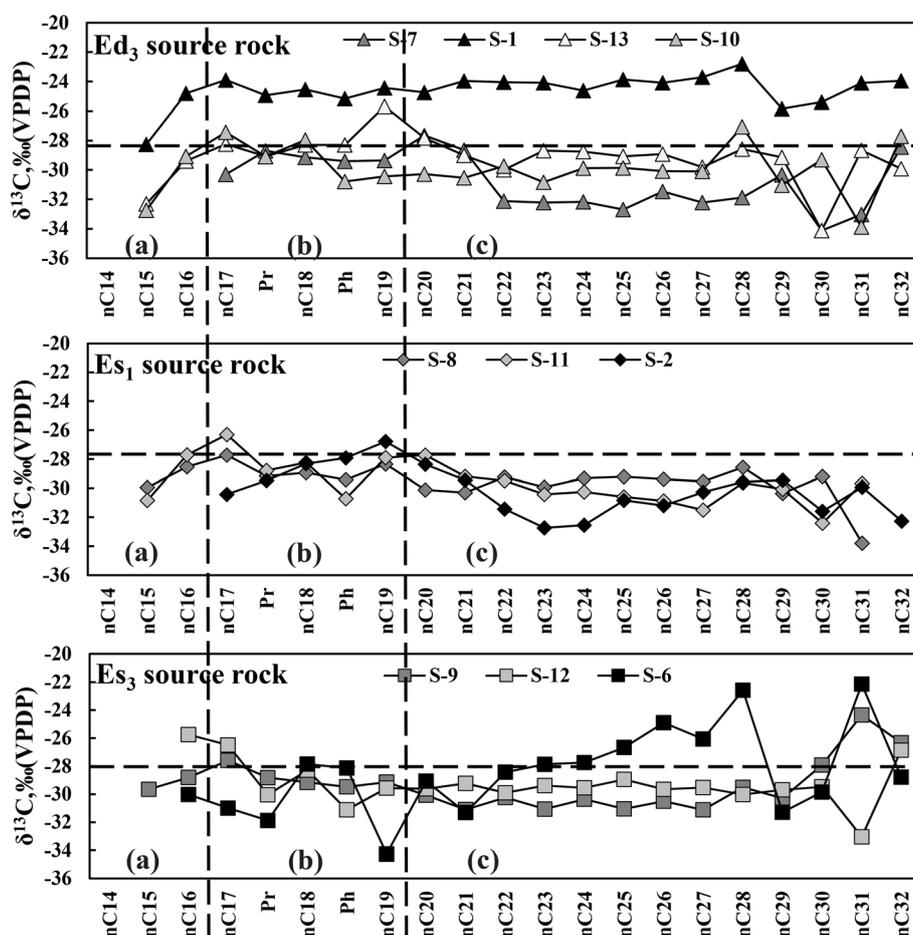

Fig. 8 Carbon isotope characteristics of *n*-alkane monomers of source rock in different layers of the Qinnan Sag.

isotopic heterogeneity, especially in the S-1 well, which displays significantly heavier carbon isotope values compared to those from the Southeast Subsag and the Eastern Fault-Step Zone. These isotope values appear to be minimally affected by carbon number, showing relatively gradual changes as the carbon number increases. This pattern is likely attributed to the proximity to a major sediment source and substantial input of terrestrial organic matter. This inference is further supported by organic petrographic observations under the microscope. For light hydrocarbons with carbon numbers less than 17, the $\delta^{13}C$ values increase progressively with increasing carbon number. The isotopic compositions of nC_{17}–nC_{19}, Pr, and Ph exhibit relatively smooth variations, while heavier hydrocarbons with higher carbon numbers show a gentle and stable isotopic trend.

For the Es_1 source rocks, the carbon isotopes of the n-alkane monomers show that the $\delta^{13}C$ values of light components with carbon numbers less than 17 become progressively heavier with increasing carbon number. nC_{17}–nC_{19}, Pr, and Ph display a V-shaped trend, with Ph exhibiting the most negative (lightest) value. In contrast, the $\delta^{13}C$ values of higher molecular weight hydrocarbons display a downward trend, becoming lighter as the carbon number increases.

For the Es_3 source rocks, the carbon isotopes of n-alkane monomers show that the $\delta^{13}C$ values of light components with carbon numbers less than 17 become progressively lighter with increasing carbon number. nC_{17}–nC_{19} and Pr and Ph exhibit a W-shaped trend, with both Pr and Ph showing relatively light values, while higher molecular weight carbon isotopes show a decreasing weight trend.

The difference in n-alkane monomer carbon isotope signatures among source rocks makes them a valuable indicator for oil–source correlation in the Qinnan Sag. By comparing the isotopic characteristics of n-alkane monomers in crude oils from different stratigraphic intervals, it was found that the crude oil from the Ed_3 and the Mz (Fig. 9) exhibit characteristics

of heavy in the early stage, a W-shaped trend in the middle segment, and an upward trend in the later segment. This pattern closely corresponds to the isotopic characteristics observed in the Es_3 source rocks.

The origin of crude oil in the Es_{12} is complex and can be further subdivided into Southeast Subsag crude oil and Liaoxi Low Uplift crude oil based on regional differences (Fig. 10). The analysis reveals that the crude oil from the Es_{12} in Southeast Subsag exhibits two distinct isotopic patterns: (1) the front part is heavier, the middle part is W-shaped, and the rear part rises, which is consistent with the characteristics of the Es_3 source rocks. (2) The front section is light, the middle segment is slightly V-shaped, and the rear section is slightly descending, which is consistent with the characteristics of the Es_1 source rocks. This indicates that the crude oil in Southeast Subsag is a mixed source. In contrast, the crude oil from the Liaoxi Low Uplift show a heavier front segment, a W-shaped middle section, and a rear segment with both upward and slightly downward trends, indicating Es_3 source dominance with minor Es_1 contribution.

Based on the above analysis, the percentage contribution of hydrocarbon source rocks to nearby areas at each layer were evaluated (Fig. 11). This intuitively reveals the oil source contribution and quality of the three sets of hydrocarbon source rocks in each region from a planar perspective. The calculation methodology is outlined as follows: the monomer carbon isotopic characteristics of n-alkanes from source rocks within the three stratigraphic intervals served as the geochemical basis for oil–source differentiation. According to the spatial distribution of crude oil samples, four calculation zones were delineated to assess the relative contributions of different source rock intervals. Within each region, the percentage contribution of each source rock interval was determined by calculating the proportion of crude oil samples whose monomer carbon
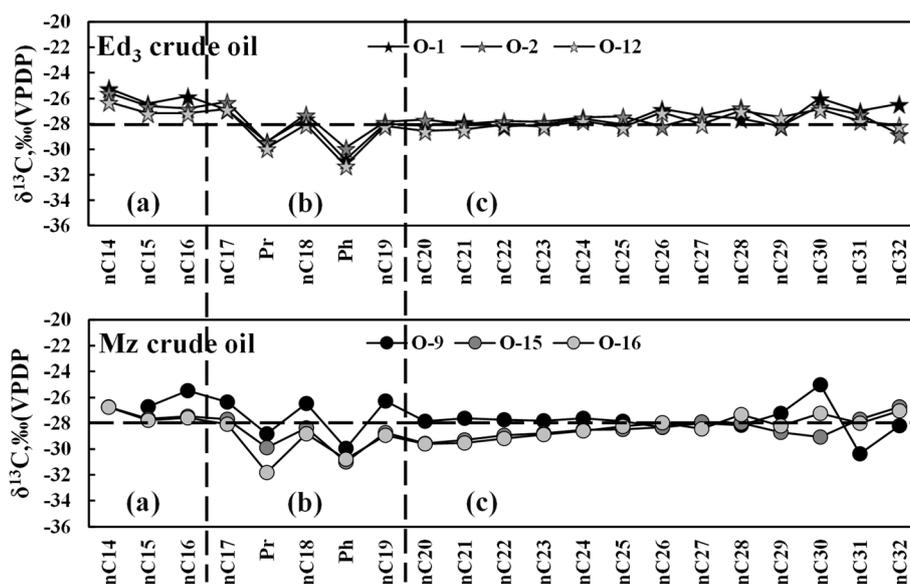

Fig. 9 Monomer isotopic characteristics of n-alkanes in Ed_3 and Mz crude oils from Qinnan Sag.
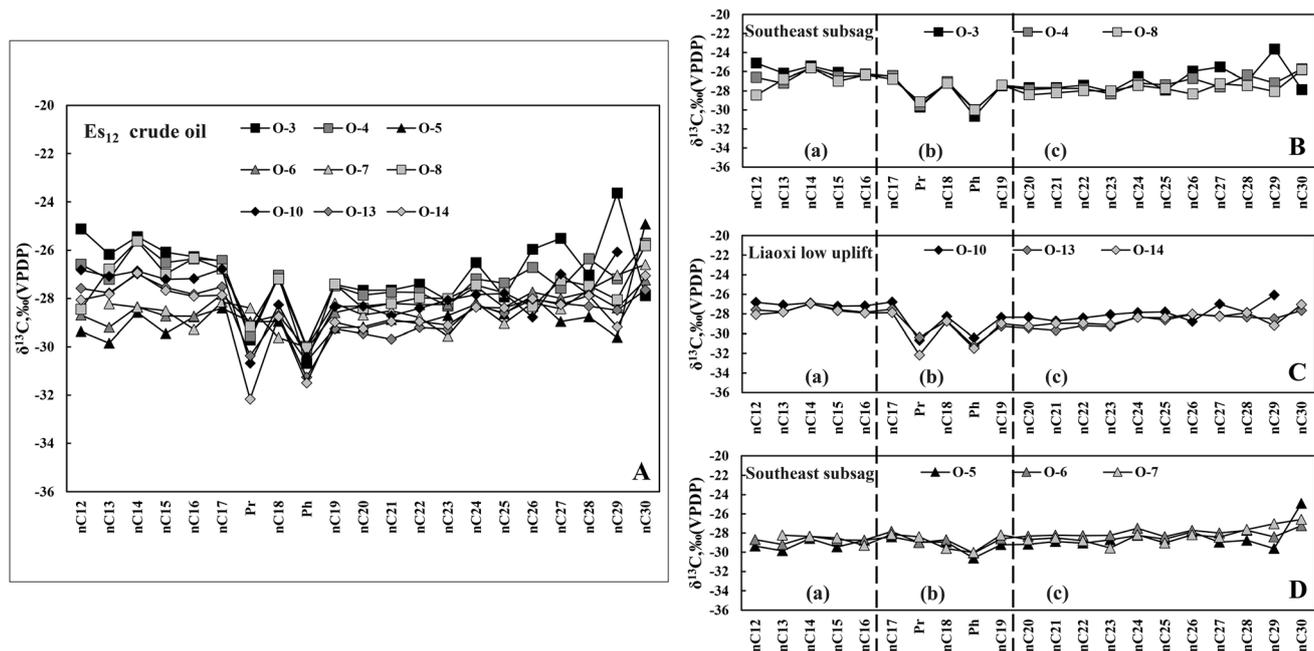
Fig. 10 Monomer carbon isotopic characteristics of *n*-alkanes in Es_{12} crude oil from Qinnan Sag. Note: (A) Es_{12} crude oil total data; (B) Es_3 characteristic crude oil data in Southeast subsag; (C) Liaoxi low rise crude oil data; and (D) Es_1 characteristic crude oil data in Southeast subsag.
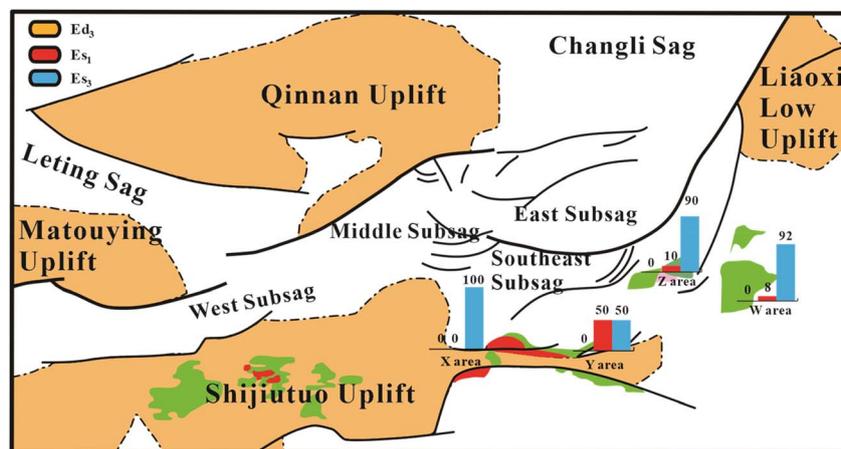

Fig. 11 Contribution characteristics of source rocks from different layers in the Qinnan Sag to crude oil in different areas.

isotope signatures matched those of a specific source rock interval.

In summary, the results of the integrated geochemical and isotopic analyses are indicative of a primary crude oil origin from the Es_3 source rocks. The Es_1 source rocks contribute notably to the crude oil in the Southeast Subsag and to a lesser extent in the Liaoxi Low Uplift. In contrast, there is no geochemical or isotopic evidence supporting a contribution from the Ed_3 source rocks.

6 Conclusions

(1) The *T*-max, HI, and microscopic composition characteristics of the Qinnan Sag suggest that the Ed_3 source rocks are primarily composed of type II_2 kerogen, while Es_1 and Es_3 source rocks are dominated by type II_1 kerogen. Maturity parameters such as *T*-max, % R_o, and molecular geochemical indicators suggest that Ed_3 source rocks are in the immature to low-mature stage, whereas Es_1 and Es_3 have reached low-mature to mature stages. According to the S_2-TOC distribution, the Es_3 is classified as high-quality source rocks, Es_1 is of relatively good quality, and Ed_3 is the least favorable.

(2) Geochemical parameters including CPI, $C_{24}TeT/C_{26}TT$, C_{27}–C_{29} regular steranes, and 4-MSI, combined with microscopic compositional analysis, suggest that the source rocks are derived from a mixed organic input of lower aquatic organisms (*e.g.*, algae) and terrestrial higher plants. In contrast, the

biomarker composition of crude oil points to a predominantly algal origin. Pr/Ph, Pr/nC_{17}, and Ph/nC_{18} ratios collectively indicate that both the source rocks and the precursor organic matter of the crude oil were deposited in a reducing lacustrine environment. Gammacerane index (G/C_{30}H) values suggest that the Ed_3 and Es_3 source rocks were formed in freshwater to brackish settings, whereas Es_1 was deposited under brackish to semi-saline conditions. The overall crude oil hydrocarbon generation parent material is in a salty to slightly salty water environment.

(3) GC-MS analysis reveals that the distributions and compositions of steranes and terpanes in both source rocks and crude oils from the Qinnan Sag are generally similar, suggesting that traditional molecular geochemical parameters possess limited effectiveness for oil–source correlation in this region. In contrast, carbon isotopes provide a relatively stable geochemical indicator that is less affected by migration or thermal maturity; furthermore, compound-specific carbon isotopes provide integrated insights into the type of organic matter, depositional environment, and hydrocarbon generation processes. These features make them a powerful tool for oil–source correlation. The monomer carbon isotopic signatures of n-alkanes demonstrate distinctive patterns across different stratigraphic source rocks: Ed_3 exhibits a "light-flat-gentle" trend from front to back; Es_1 is characterized by a "light front-moderate V-shaped middle-light rear decline"; while Es_3 shows a "heavy front-W-shaped middle-rising rear" pattern.

(4) Crude oil in the Qinnan Sag shows relatively high thermal maturity, and there is no geochemical or isotopic evidence indicating a contribution from the Ed_3 source rocks. The isotopic characteristics of crude oils from Ed_3 and Mz strata resemble those of Ed_3 source rocks, while the Es_{12} crude oil exhibits more complex origins. Based on regional differences, Es_{12} crude oil can be divided into two groups: crude oil from the Southeast Subsag shows mixed-source characteristics derived from both Es_1- and Es_3-type source rocks; Liaoxi-Low-Uplift crude oil exhibits characteristics with contributions from the Es_3 main type and a small amount of Es_1.

Data availability

The raw data generated during this study and the raw dataset used to generate research results are stored in the author's personal database. Interested parties can contact the author to obtain them. These data have been anonymized and/or pseudonymized to ensure compliance with privacy regulations. The processed and analyzed data are stored in the author's personal database, and interested parties can contact the author. Part of the data processing was carried out using the software "Data Analysis", as described in Sections 4.2–4.4 of the manuscript. More detailed information can be obtained by consulting the author *via* email. All data used to support the results of this study are included in this article. Unless otherwise stated in the manuscript, any interested party may replicate our experiments and/or analyze the data using standard statistical tools and protocols.

Author contributions

Xukai Shi: writing – original draft. Xiaomin Xie: writing – review & editing.

Conflicts of interest

The authors declare that they have no known competing financial interests or personal relationships that could have appeared to influence the work reported in this paper.

Acknowledgements

References

1 J. F. Qi and Q. Yang, Cenozoic structural deformation and dynamic processes of the Bohai Bay basin province, China, *Mar. Petrol. Geol.*, 2009, **27**(4), 757–771.

2 Y. L. Jiang, S. M. Su, H. Liu, Y. S. Wang and X. J. Cui, Differential hydrocarbon enrichment of the Paleogene and its main controlling factors in the Bohai Bay Basin, *Oil Gas Geol.*, 2020, **41**(02), 248–258.

3 L. Zhang, D. Y. Wang, X. T. Zhang, Y. M. Liu and W. Xu, The Controlling Factors of the High-quality Mixed Reservoirs in QHD29-2E Structure, Bohai Sea, *Acta Sedimentol. Sin.*, 2019, **37**(01), 200–211.

4 L. Zhang, X. T. Zhang, Y. M. Liu, R. Han and G. C. Wei, Evidence of deep fluid and its influence on gas reservoiring in Bohai Sea: Cast study of QHD29-2/2E Oilfield, *Nat. Gas Geosci.*, 2021, **32**(05), 633–644.

5 Y. A. Xue, X. J. Pang, Y. W. Hao and C. Feng, Genesis of High-Quality Mixed Rock Reservoir and Its Exploration Significance in Es1 around Southeast Margin of Qinnan Sag, Bohai Sea, *Earth Sci.*, 2020, **45**(10), 3527–3542.

6 C. M. Niu, F. L. Wang, G. M. Tang, G. Yan and G. X. Zhao, Evaporative fractionation and biodegradation impacts on a complex petroleum system: QHD29-2 oil field, Bohai Sea area, *Pet. Geol. Exp.*, 2018, **40**(03), 381–388.

7 X. B. Zhuang, H. Y. Zou, N. Li, Y. Y. Yang and H. F. Sun, Characteristics of source rock and new region of oil and gas exploration in Qinnan sag, *Fault-Block Oil Gas Field*, 2011, **18**(02), 146–149.

8 D. S. Shi, M. W. Li, X. Q. Pang, D. X. Chen, S. W. Zhang, Y. S. Wang and Q. Jin, Fault-fracture mesh petroleum plays in the Zhanhua Depression, Bohai Bay Basin: Part 2. Oil-source correlation and secondary migration mechanisms, *Org. Geochem.*, 2005, **36**(2), 203–223.

9 S. D. Jin, H. Y. Cao, H. Wang and S. B. Chen, The Paleogene multi-phase tectono-sedimentary evolution of the syn-rift stage in the Nanpu Sag, Bohai Bay Basin, East China, *Energy Explor. Exploit.*, 2018, **36**(6), 1519–1545.

10 H. X. Li, B. Liu, X. Z. Liu, L. N. Meng, L. J. Cheng and H. X. Wang, Mineralogy and inorganic geochemistry of the Es4 shales of the Damintun Sag, northeast of the Bohai Bay Basin: Implication for depositional environment, *Mar. Petrol. Geol.*, 2019, **110**, 886–900.

11 S. Chen, R. Zhao, C. W. Chen, H. Wang, J. H. Ma, T. H. Gong and Z. H. Yu, Tectono-sedimentary evolution of the Paleogene Qikou Sag, Bohai Bay Basin, NE China, *Mar. Petrol. Geol.*, 2023, **148**, 106057.

12 C. C. Yang, R. Guo, F. M. Wang, Z. Zhang and X. G. Pei, Quantitative prediction of TOC in source rocks of the Member 3 of Shahejie Formation in Qinnan Depression, Bohai Sea, China, *J. Chengdu Univ. Technol.*, 2019, **216**(05), 549–557.

13 N. Arif and F. Tahira, Geochemistry of Cretaceous rocks, Pakistan: II. Interpretation of source, depositional environment and lithology of organic matter, *Pet. Sci. Technol.*, 2017, **35**(10), 937–946.

14 I. Samra, F. Tahira, I. Faiza and N. Arif, Geochemical characteristics and hydrocarbon potential of Cretaceous Upper Shale Unit, Lower Indus Basin, Pakistan, *Pet. Sci. Technol.*, 2022, **40**(3), 257–269.

15 Q. Wang, F. Hao, C. G. Xu, Y. B. Wang and H. Y. Zou, Geochemical characterization of QHD29 oils on the eastern margin of Shijiutuo uplift, Bohai Sea, China: Insights from biomarker and stable carbon isotope analysis, *Mar. Pet. Geol.*, 2015, **64**(03), 266–275.

16 F. Hao, X. H. Zhou, Y. Zhu and Y. Yang, Mechanisms for oil depletion and enrichment on the Shijiutuo uplift, Bohai Bay Basin, China, *AAPG Bull.*, 2009, **93**(8), 1015–1037.

17 X. K. Shi, Y. Liu, D. Y. Wang, F. Liu, F. L. Wang, Z. G. Wen, X. M. Xie, Y. Z. Wu and Z. D. Lu, Geochemical characteristics of crude oil in the eastern of Qinnan sag, Bohai Bay Basin, Eastern China, *Front. Earth Sci.*, 2022, **10**, DOI: 10.3389/feart.2022.998152.

18 J. P. Bao, C. S. Si, X. C. Jiang, R. H. Zhang, C. S. Zhu, L. Huang, L. Q. Ma and P. W. Wang, The Bimodal Distributions of n-alkanes in the Post-mature Marine Source Rocks and Solid Bitumen from the Northern Guizhou Depression, *Acta Sedimentol. Sin.*, 2016, **34**(01), 181–190.

19 R. X. Yang, W. Y. Wang, M. K. Cai, D. D. Wang and X. G. Luo, A study of tectonic framework of the Qinnan sag in Bohai Basin and its adjacent areas based on satellite gravity anomalies, *Geophys. Geochem. Explor.*, 2023, **47**(03), 584–596.

20 W. L. Shi, H. Y. Li, L. Mao, H. F. Yang, L. X. Chen and H. B. Yu, Hydrocarbon Geological Characteristics and Exploration Potential of Qinnan Depression in Offshore Area of Bohai sea. China, *Pet. Exp.*, 2014, **94**(05), 32–40.

21 W. Li, Y. J. Xu, Z. F. Liu, Y. C. Li and W. Q. Zhu, Influence of mantle-derived CO2 on hydrocarbon accumulation in Qinhuangdao 29 tectonic zone, Bohai Sea, *Oil Gas Geol.*, 2023, **44**(02), 418–428.

22 S. W. Cai, D. H. Zhou, D. Y. Wang, J. S. Zhang, Z. Zhang and Y. Li, Tectonic development characteristics and favorable exploration direction of Qinnan sag in Bohai Bay Basin, *Acta Pet. Sin.*, 2019, **40**(05), 532–541.

23 L. Liu, H. D. Chen, Y. J. Zhong, J. Wang, X. F. Du and H. Zou, Depositional architectures and sedimentation processes in strike-slip extensional basins: Examples from the Oligocene of the Liaodong Bay Sub-basin, Bohai Bay Basin, China, *Mar. Petrol. Geol.*, 2020, **123**, 104788.

24 H. Liu, X. P. Liu, G. Y. Liu, G. Y. Li, J. W. Wang, Y. L. Gao, B. Sun, J. K. Hou, H. X. Liu and X. J. Sun, Sedimentary environment controls on the lacustrine shale lithofacies: A case study from the Nanpu depression, Bohai Bay Basin, *Geoenergy Sci. Eng.*, 2023, **225**, 211704.

25 C. X. Zhu, F. J. Jiang, P. Y. Zhang, T. Hu, Y. Liu, T. W. Xu, Y. X. Zhang, Q. Deng, Y. S. Zhou, H. Xiong and Z. Z. Song, Identification of effective source rocks in different sedimentary environments and evaluation of hydrocarbon resources potential: A case study of paleogene source rocks in the Dongpu Depression, Bohai Bay Basin, *J. Petrol. Sci. Eng.*, 2021, **201**(1), 108477.

26 C. W. Liu, X. C. You, H. Li, S. B. Li, H. Chen, Z. S. Wang, M. N. Chen and Z. H. Li, Geochemical characteristics and hydrocarbon generation potential of Lucaogou Formation source rocks in Fukang Sag, Junggar Basin, *Pet. Geol. Exp.*, 2023, **45**(02), 338–346.

27 M. L. Deng, N. Wang, X. Q. Li, R. T. Chen, Y. Liu and Y. H. Xu, Geochemical characteristics and sedimentary environment of source rocks of the third member of Paleogene Shahejie Formation in central Laizhouwan Sag, Bohai Sea, *Lithol. Reservoirs*, 2023, **35**(1), 49–62.

28 Y. W. Gao, S. Y. Hao, Q. Wang, W. B. Wang, S. J. Jiang, Q. X. Fan, Z. J. Chen and Y. Zhou, Geochemical characteristics and hydrocarbon resources potential of source rocks in Babei Sag, Yingen-Ejinaqi Basin, *Oil Gas Geol.*, 2022, **43**(06), 1445–1458.

29 Z. D. Lu, Y. Liu, Z. L. Chen, Y. P. Fan, Z. G. Wen, Y. H. Xu, J. Niu, Y. J. Tian, B. Liu, X. M. Xie and W. Xie, An improved method and indications for the compound specific isotopic analysis of hopanes in source rock extracts, *Pet. Geol. Exp.*, 2022, **44**(02), 288–294.

30 J. P. Bao, C. H. Ni, C. S. Zhu, Z. W. Zhan, X. C. Jiang and X. Shen, Carbon isotope compositions of individual alkanes in highly mature source rocks from Northern Guizhou Depression, *Pet. Geol. Exp.*, 2019, **41**(06), 838–848.

31 E. Gelpi, J. Schneider, J. Mann and J. Oro, Hydrocarbons of geochemical significance in microscopicalgae, *Phytochemistry*, 1970, **9**(3), 603–612.

32 S. R. Jacobson, J. R. Hatch, S. C. Teerman and R. A. Askin, Middle Ordovician Organic Matter Assemblages and Their Effect on Ordovician-Derived Oils, *AAPG Bull.*, 1988, **72**(9), 1090–1100.

33 M. Harouna, J. D. Pigot and R. P. Phlp, Burial history and thermal maturity evolution of the Termit Basin, Niger, *J. Petrol. Geol.*, 2017, **40**(3), 277–297.

34 M. Leila, A. Awadalla, A. Farag and A. Moscariello, Organic geochemistry and oil-source rock correlation of the

Cretaceous succession in West Wadi El-Rayan (WWER) concession: Implications for a new Cretaceous petroleum system in the north Western Desert, Egypt, *J. Petrol. Sci. Eng.*, 2022, **219**, 111071.

35 K. Pehr, A. A. Baczynski, A. Bekker, A. Hoffmann, K. H. Freeman, S. W. Poulton and G. D. Love, Compound-specific carbon isotope measurements of individual lipid biomarkers from immature Ediacaran rocks of Baltica, *Org. Geochem.*, 2023, **182**, 104641.

36 C. Z. Li, F. H. Xu, X. B. Huang, T. Jiang, G. S. Xu and P. Guo, Migration directions of crude oils from multiple source rock intervals based on biomarkers: A case study of Neogene reservoirs in the Bodong Sag, Bohai Bay Basin, *Energy Rep.*, 2022, **8**, 8151–8164.

37 K. E. Peters and J. M. Moldowan, *The Biomarker Guide: Interpreting Molecular Fossils in Petroleum and Ancient Sediments*, ed. N. J. Englewood Cliffs, Prentice Hall, 1993, vol. 30, 5, pp. 30–2690.

38 J. L. Zhou and M. Zhang, Geochemical characteristics of crude oil saturated hydrocarbons in the central structural zone of Lishu fault depression, Songliao Basin, *Liaoning Chem. Ind.*, 2021, **50**(02), 254–258.

39 C. J. Wu, M. F. Zhang, Y. Liu, R. Chen, D. M. Xiong and J. C. Tuo, Geochemical characteristics of Paleozoic shale in Sichuan Basin and their gas content features, *J. China Coal Soc.*, 2013, **38**(05), 794–799.

40 Q. Jin, Q. J. Hou, F. Q. Cheng, S. L. Wang, R. C. Zhang and F. L. Wang, Evaluation method of effective source rock in mature exploration area: a case study of Liaodong Bay, *Acta Pet. Sin.*, 2019, **40**(03), 257–267.

41 N. Liu, N. S. Qiu, C. Cai, Z. M. Li, Y. J. Wang, Y. X. Jiao, T. Gao, H. L. Sun and M. Lu, Geochemical characteristics and natural gas-oil-source correlation of the Shulu depression in the Jizhong Subbasin, Bohai Bay Basin, eastern China, *J. Petrol. Sci. Eng.*, 2022, **216**, 110831.

42 K. E. Peters, J. M. Moldowan, M. Schoell and W. B. Hempkins, Petroleum isotopic and biomarker composition related to source rock organic matter and depositional environment, *Org. Geochem.*, 1986, **10**, 17–27.

43 W. K. Seifert and J. M. Moldowan, Applications of steranes, terpanes and monoaromatics to the maturation, migration and source of crude oils, *Geochem. Cosmochim. Acta*, 1978, **42**(1), 77–95.

44 L. I. P. Dzou, R. A. Noble and J. T. Senftle, Maturation effects on absolute biomarker concentration in a suite of coals and associated vitrinite concentrates, *Org. Geochem.*, 1995, **23**, 681–697.

45 J. M. Hunt, *Petroleum Geochemistry and Geology*, W. H. Freeman, New York, 1996, pp. 466–467.

46 F. R. Aquino Neto, A. Restle, J. Connan, P. Albrecht and G. Ourisson, Novel tricyclic terpanes (C19, C20) in sediments and petroleums, *Tetrahedron Lett.*, 1983, **23**(19), 2027–2030.

47 M. A. Barnes and W. C. Barbers, Oxic and anoxic diagenesis of diterpenes in lacustrine sediments, *Advances in Organic Geochemistry*, John Wiley & Sons, New York, 1983, pp. 289–298.

48 P. A. Meyers, Applications of organic geochemistry to paleolimnological reconstructions: a summary of examples from the Laurentian Great Lakes, *Org. Geochem.*, 2003, **34**(2), 261–289.

49 J. M. Moldowan, J. Dahl, B. J. Huizinga, F. J. Fago, L. J. Hickey, T. M. Peakman and D. W. Taylor, The molecular fossil record of oleanane and its relation to angiosperms, *Science*, 1994, **265**(5173), 768–771.

50 W. K. Seifert and J. M. Moldowan, Paleoreconstruction by biological markers, *Geochem. Cosmochim. Acta*, 1981, **45**, 783–794.

51 A. S. Mackenzie, C. Beaumont and M. K. Dan, Estimation of the kinetics of geochemical reactions with geophysical models of sedimentary basins and applications, *Org. Geochem.*, 1984, **6**, 875–884.

52 J. M. Moldowan and F. J. Fago, Structure and significance of a novel rearranged monoaromatic steroid hydrocarbon in petroleum. Geochem. Cosmochim, *Acta*, 1986, **50**, 343–351.

53 R. Alexander, R. I. Kagi and G. W. Woodhouse, Geochemical correlation of windalia oil and extracts of winning group (cretaceous) potential source rocks, barrow subbasin, western Australia, *AAPG Bull.*, 1981, **65**(2), 235–250.

54 J. S. Sinninghe Damste, F. Kenig, M. P. Koopmans, J. Köster, S. Schouten, J. M. Hayes and J. W. Leeuw, Evidence for gammacerane as an indicator of water column stratification, *Geochem. Cosmochim. Acta*, 1995, **59**(9), 1895–1900.

55 K. E. Peters, A. E. Cunningham, C. C. Walters, J. G. Jiang and Z. A. Fan, Petroleum systems in the jiangling-dangyang area, jianghan basin, China, *Geochemistry*, 1996, **24**(10–11), 1035–1060.

56 H. Q. Sun, Exploration practice and cognitions of shale oil in Jiyang depression, *China Petrol. Explor.*, 2017, **22**(04), 1–14.

57 P. Yang, Y. Xie, Z. J. Wang, Q. D. Du and J. H. Liu, Geochemical characteristics and oil source correlation of Dengying formation paleo-reservoir in Jinsha, *Geochemistry*, 2012, **41**(05), 452–465.

58 E. T. Li, C. C. Pan, S. Yu, X. D. Jin and J. Z. Liu, Interaction of coal and oil in confined pyrolysis experiments: Insight from the yields and carbon isotopes of gas and liquid hydrocarbons, *Mar. Petrol. Geol.*, 2016, **69**, 13–37.

59 Q. Y. Jin, Genesis types and accumulation characteristics of crude oil in southeast slope of Weixinan Depression, Beibuwan Basin, *Lithol. Reservoirs*, 2020, **32**(01), 11–18.

60 F. Diao, J. W. Wang, X. N. Chen, Z. J. Wang and Y. C. Zhang, Correlation of oils and source rocks and genesis of high wax oils in Gaoshangpu area, Nanpu Sag, Bohai Bay Basin. Pet, *Geol. Expt.*, 2020, **42**(01), 117–125.